



HAL
open science

Transition from simple to complex contagion in collective decision-making

Nikolaj Horsevad, David Mateo, Robert Kooij, Alain Barrat, Roland Bouffanais

► **To cite this version:**

Nikolaj Horsevad, David Mateo, Robert Kooij, Alain Barrat, Roland Bouffanais. Transition from simple to complex contagion in collective decision-making. *Nature Communications*, 2022, 13 (1), pp.1442. 10.1038/s41467-022-28958-6 . hal-03612211

HAL Id: hal-03612211

<https://hal.science/hal-03612211>

Submitted on 17 Mar 2022

HAL is a multi-disciplinary open access archive for the deposit and dissemination of scientific research documents, whether they are published or not. The documents may come from teaching and research institutions in France or abroad, or from public or private research centers.

L'archive ouverte pluridisciplinaire **HAL**, est destinée au dépôt et à la diffusion de documents scientifiques de niveau recherche, publiés ou non, émanant des établissements d'enseignement et de recherche français ou étrangers, des laboratoires publics ou privés.

1 Transition from simple to complex contagion in 2 collective decision-making

3 **Nikolaj Horsevad**^{1,*}, **David Mateo**², **Robert E. Kooij**^{3,4}, **Alain Barrat**^{5,6}, and **Roland**
4 **Bouffanais**^{1,†}

5 ¹University of Ottawa, Ottawa, Canada

6 ²Kido Dynamics, Lausanne, Switzerland

7 ³Delft University of Technology, Delft, The Netherlands

8 ⁴The Netherlands Organization for Applied Scientific Research (TNO), The Hague, The Netherlands

9 ⁵Aix Marseille Univ, Université de Toulon, CNRS, CPT, Turing Center for Living Systems, Marseille, France

10 ⁶Tokyo Tech World Research Hub Initiative (WRHI), Tokyo Institute of Technology, Tokyo, Japan

11 *nikolajhorsevad@gmail.com

12 †roland.bouffanais@uottawa.ca

13 **ABSTRACT**

How does the spread of behavior affect consensus-based collective decision-making among animals, humans or swarming robots? In prior research, such propagation of behavior on social networks has been found to exhibit a transition from simple contagion—i.e, based on pairwise interactions—to a complex one—i.e., involving social influence and reinforcement. However, this rich phenomenology appears so far limited to threshold-based decision-making processes with binary options. Here, we show theoretically, and experimentally with a multi-robot system, that such a transition from simple
14 to complex contagion can also be observed in an archetypal model of distributed decision-making devoid of any thresholds or nonlinearities. Specifically, we uncover two key results: (i) the nature of the contagion—simple or complex—is tightly related to the intrinsic pace of the behavior that is spreading, and (ii) the network topology strongly influences the effectiveness of the behavioral transmission in ways that are reminiscent of threshold-based models. These results offer new directions for the empirical exploration of behavioral contagions in groups, and have significant ramifications for the design of cooperative and networked robot systems.

15 **Introduction**

16 Complex systems, be them natural or artificial, operate on the basis of a particular connectivity between
17 constituting elements, which orchestrates the execution of specific dynamical processes. Such a high-level
18 abstraction encompasses wildly different systems giving rise to a range of emergent behaviors, such as fish
19 schooling^{1–3}, social opinion formation⁴, disease spreading⁵, cascading failures in power grids^{6,7}, target
20 tracking by swarm robotic systems^{8,9}, etc. Such collective dynamics have been found to be crucially
21 dependent on the underlying network topology^{2,3,5,10–15}, which conditions the efficient transmission of
22 behavioral change.

23 The propagation of state changes within a social system—or an engineered networked one—has been
24 acknowledged to be akin to a contagion process, which can be either ‘simple’ or ‘complex’^{13,16–19}. With
25 a simple contagion, the behavior propagates through a single exposure or interaction. On the other hand, if
26 social reinforcement is required—following Centola and Macy’s definition¹³: “if its transmission requires
27 an individual to have contact with two or more sources of activation”—the contagion is said to be complex.

28 Numerous models of behavioral propagation in networked systems (including social ones) have been

29 considered over the years. Threshold models have been the predominant modeling framework used to
30 characterize a wide range of complex contagion processes, such as the adoption of technological innova-
31 tions⁴ or preventative health measures²⁰, and the spread of misinformation on social media^{19,21} (Note that
32 complex-like contagions are also observed with stochastic models of epidemic-like processes^{22–25}). The
33 growing interest in threshold models can be traced to their mathematical simplicity, their paradigmatic
34 nature and their success in modeling the spread of behaviors in various social settings^{4,13,16,26}. These
35 deterministic models assume that agents can be in two states (inert or activated), and that a particular agent
36 becomes activated if a fraction of its neighbors (in the network sense) larger than a given threshold are
37 themselves activated^{17,27}. These threshold models fit perfectly Centola & Macy’s original definition of a
38 complex contagion, whereby a transition from simple to complex contagion takes place when increasing
39 the threshold beyond a value corresponding to having more than one activated neighbor^{13,16,17}. However,
40 the key concept of activation may not be as straightforward when considering models lacking a threshold,
41 which can become an issue when trying to use the existing definition of a complex contagion.

42 Here, we show theoretically and experimentally that such a transition from simple to complex contagion,
43 as originally identified in threshold-based models, can also be exhibited by another general class of
44 collective decision-making processes; specifically, a class of models based on consensus and devoid of
45 any thresholds or nonlinearities. Using a new way of characterizing complex contagions, we uncover
46 their existence in consensus-based dynamics. Specifically, we shed a new light on some fundamental
47 mechanisms underpinning networked systems, which may support the study of a vast range of collective
48 behaviors in both the animal and social worlds.

49 Unsurprisingly, the network topology plays a pivotal role in this study^{2,3,10–13,15,16}. It is known that it
50 strongly affects both spreading types in threshold models, albeit in fundamentally different ways. While
51 simple contagions are enhanced by short network distances⁵, complex ones are amplified by high levels of
52 clustering^{4,5,14,16}. Within the framework of threshold models, the behavior or state being transmitted is
53 of a binary nature: ‘active’ or ‘inactive’. This simplification clearly facilitates the tracking of behavioral
54 cascades from a source (or multiple sources) to the entire system (or parts of the system). This feature
55 serves well the purpose of studying collective decision-making processes involving two options, such as
56 voting, adoption of innovations, binary opinion dynamics^{4,20}. However, numerous collective decisions are
57 more complex and involve a continuum of options rather than just a binary set^{28–30}. A full understanding
58 of the influence of network metrics on consensus-based decision-making involving behavioral propagation
59 and/or external perturbations to the consensus is lacking. Such knowledge would help gain insight into the
60 disturbed collective dynamics of social and animal groups, e.g., when responding to a predator’s attack or
61 to misleading information on social networks.

62 Biologists have indeed recently acknowledged the profound similarities between human and animal
63 social behaviors. For instance, Sosna et al. recently reported a study on the “fear response” of a school
64 of fish collectively making fast decisions under risky conditions³. They found that the properties of
65 the network (their “social connectivity”) are the primary factors responsible for the high collective
66 responsiveness of the school in terms of number of behavioral cascades and their sizes. Furthermore,
67 Firth¹⁸ has made the case that complex contagions might be key to explaining some specific collective
68 animal dynamics, especially those with socially transmittable behaviors. In the case of direct behavioral
69 transmission in mobile animal groups—schooling fish, flocking birds, swarming insects^{31–34}—a full
70 understanding of the nature of the propagation is still lacking^{2,3}. The markedly fast spread of behaviors
71 within animal groups—such as waves of response, evasive maneuvers in schools of fish^{2,3,11,35}, and
72 collective turns in flocks of starlings³⁶—has been a source of inquiry for a long time³⁵. Recent large-
73 scale empirical evidence with fish and birds have revealed the intricate patterns of interaction among
74 individuals^{2,3,36–39}, which underpin the behavioral cascades throughout the group. A key element to these

75 inter-agent interactions is alignment—metric or topological—that introduces a consensus component to
76 the collective decision-making process. Unlike binary threshold-based models, such orientation-consensus-
77 based ones do not lend themselves well to the tracking of behavioral cascades given the non-binary
78 nature of the state-variable. Moreover, as with all ethological results, even if it is possible to modify the
79 interaction among agents in some ways³, it is virtually impossible to fully control all aspects of it.

80 However, biologists have started using robotic agents in place of animals to be able to measure and
81 quantify some features of interest^{40,41}. Hence, by following a similar approach with a multi-robot system,
82 one could compare the effectiveness of the social transmission of information when changing the local
83 interaction rule, i.e. when changing the topology of the interaction network.

84 Here, we specifically consider a collective decision-making process reminiscent of a group escape
85 response. Using the leader-follower consensus (LFC) dynamics—a particular instance of the general
86 control-theoretic framework of the Taylor model^{30,42,43}—we are able to study the behavioral contagion
87 within a group of networked agents driven by a single leader acting as a stimulus of tunable frequency^{11,12}.
88 With this linear-time invariant (LTI) dynamics, by varying the network topology—specifically the cluster-
89 ing coefficient, average shortest path and Kirchhoff index—we observe that slow-paced (resp. fast-paced)
90 stimuli propagate in ways reminiscent of a simple (resp. complex) contagion. Furthermore, we uncover a
91 transition from simple to complex contagion when varying the pace of the stimulus—i.e. its frequency.
92 This transition is made apparent by measuring the effectiveness of the behavioral propagation—quantified
93 here by means of the concept of collective frequency response¹²—when varying the topological features
94 of the interaction networks (e.g., clustering coefficient, average shortest path, etc.). In addition, using a
95 robotic experimental test-bed comprising 10 networked agents performing an angular heading consensus
96 similar to those observed in collective turns of flocking starlings³⁹, we unambiguously confirm that the
97 behavioral propagation has the features of a complex contagion when driven by fast-paced stimuli.

98 These results have far-reaching implications for several reasons. First, they extend the concept of
99 transition from simple to complex contagion—heretofore limited to binary threshold-based models^{16,17}—
100 to the continuous class of consensus-based models. It is worth highlighting that the original linear threshold
101 model (LTM) with binary options has been extended to a continuous threshold model (CTM) of cascade
102 dynamics, which involves nonlinearities and a threshold⁴⁴. However, no evidence of a transition from
103 simple to complex contagion has been reported for the CTM. Second, these results reveal that the nature
104 of the contagion—simple or complex—is directly related to the type of behavior spreading, and more
105 specifically to the pace of its intrinsic dynamics—e.g., slow external perturbations vs. collective startle
106 response. Lastly, the insights gained from this study could offer new directions for biologists and social
107 scientists to explore and experiment with animal and human groups respectively. They could also be
108 harnessed to improve the design and robustness of engineered networked systems (e.g. Internet of Things,
109 sensor networks, swarm robotics).

110 Results

111 Polarization speed in threshold models

Complex contagions have been originally uncovered and studied using the archetypal LTM^{13,16,17,27}, where nodes become active when the fraction of their active neighbors crosses a certain threshold θ . Specifically, the LTM dictates that for any agent i , the binary state-variable $s_i(t)$ is updated according to

$$s_i(t+1) = \begin{cases} 1 & \text{if } \langle s_j(t) \rangle_{j \sim i} > \theta, \\ 0 & \text{otherwise,} \end{cases} \quad (1)$$

112 where $\langle \cdot \rangle_{j \sim i}$ is the average over all neighbors of i (Methods). Significant attention has been dedicated to
 113 understanding the interplay between θ and network topology for global cascades to occur (i.e. yielding
 114 an activation of 99% of nodes)¹³. It has been repeatedly reported that complex contagions spread “faster
 115 and further”^{16,20} on highly clustered networks, as compared to simple contagions^{13,16,45}. It is worth
 116 stressing that the investigation of this important statement remains limited to the long-term dynamics of
 117 global cascades⁴⁶. On the other hand, the early dynamics of contagion affecting a smaller fraction of
 118 nodes—say cascades of 30% activated nodes, which is still macroscopic—has been relatively overlooked.
 119 There has been no attempt to relate the actual speed of contagion with the transition from simple to
 120 complex contagion for incomplete—i.e., non-global—cascades. This speed of contagion, also known
 121 as diffusion speed, is the number of infected nodes per unit time and is increasingly recognized as an
 122 important indicator of the contagion dynamics^{11,46–49}.

123 A useful metric to analyze this is given by the so-called polarization speed $v = (P(t) - P(0))/t$ at
 124 instant t , where $P(t)$ measures the polarization of the system (Methods). This quantity gives an indication
 125 of the speed at which a random activator node and its neighbors can activate a given fraction of nodes
 126 (here 30%; Methods and Supplementary Fig. S1 for other fractions)^{11,17,22,27}. Here, we consider this
 127 polarization speed, which is identical to the average speed of diffusion considered in Ref.⁴⁶ and is also
 128 somehow related to the concepts of spreading speed, half prevalence time, or time until half the network is
 129 infected^{48,50,51}, and we study how it relates to some network descriptors used for the study of the spread
 130 of misinformation in temporal network epidemiology⁵².

131 Following in the footsteps of Centola & Macy, we use their version of the LTM¹⁶ to study the transition
 132 from simple to complex contagion. Simple contagions are observed in LTMs with low thresholds θ , which
 133 lead to an increased spreading rate on networks with smaller values of the average shortest path ℓ ^{5,45}.
 134 As θ increases, the contagion becomes complex and for the spreading process to endure, the network
 135 must possess a sufficiently high value of the clustering coefficient C ^{13,17}. Here, we consider the classical
 136 small-world Watts–Strogatz (WS) networks⁵, which are constructed on the basis of a single free parameter,
 137 namely the rewiring probability p . By varying p , we can effectively tune C , ℓ , or the Kirchhoff index
 138 R_g of the network (Methods). The Kirchhoff index $R_g = N \sum_{i=2}^N \lambda_i^{-1}$, is a distance metric based on the
 139 eigenvalues $0 = \lambda_1 < \lambda_2 < \dots < \lambda_N$ of the Laplacian matrix⁵⁹ (Methods).

140 The variations of the polarization speed v with θ are reported in Fig. 1. At low threshold, the
 141 polarization speed increases when ℓ decreases (and C decreases as well), which is characteristic of simple
 142 contagions (Fig. 1(a)). At higher θ values, this trend is inverted and we retrieve the well-known complex
 143 contagion phenomenology in which v increases with C (and also with ℓ). These trends can also be
 144 appreciated by observing the particular network topology corresponding to the purple curve (high C , ℓ and
 145 R_g) in Fig. 1(a). It goes from producing the worst performing simple contagion (out of the 4 topologies
 146 considered here) at low θ , to generating the best performing complex contagion at higher threshold values.
 147 As expected, the transition region corresponds to intermediate values of the threshold such that the ordering
 148 of the different networks does not reveal an unambiguous simple or complex contagion. It is worth noting
 149 that highly clustered networks can sustain a complex contagion at higher thresholds compared to the more
 150 rewired networks, which lack ample clustering to sustain spreading¹³.

151 To analyze this transition, we calculate the Spearman’s correlation coefficient r_s between the po-
 152 larization speed v and each network metric $\chi \in \{C, \ell, R_g\}$, for each threshold value θ (Methods and
 153 Supplementary Fig. S2). There is a marked transition from $r_s \approx -1$ for $\theta < 0.1$, to $r_s \approx +1$ when $\theta > 0.28$
 154 (Fig. 1b). These thresholds mark the cutoff of purely simple and complex contagion—used to draw the
 155 shaded regions in Fig. 1a—with the transition region in between experiencing a more complex interplay
 156 of the network parameters and the resulting polarization speed. Note that the correlation between the three
 157 network parameters and the polarization speed are extremely similar, owing to the well-known fact that the

158 WS network model has only one free parameter (the rewiring probability p ; see Ref.⁵). These results are in
 159 good agreement with other observations of this transition^{5,16,17,45}, thereby suggesting that v , characteristic
 160 of the early contagion dynamics, is both an adequate and effective indicator of the nature—simple or
 161 complex—of the behavioral propagation.

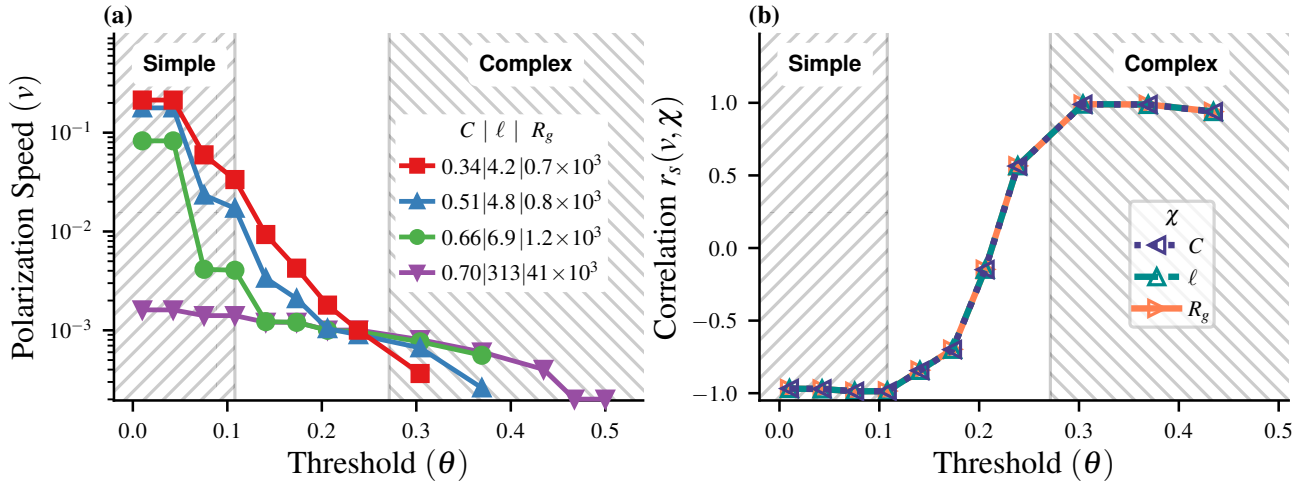


Figure 1. Linear threshold model on WS networks of $N = 10,000$ nodes, with fixed average degree $\langle k \rangle = 16$ and uniform threshold θ . Initially a single randomly selected seed node and its neighbors are activated. (a) Average polarization speed v when the cascade size is 30% active nodes on the network, with lines stopping prematurely if the fraction is never reached, shown for a representative set of network metrics (Supplementary Fig. S1 for other cascade sizes). The WS rewiring probability p is used to generate network samples having specific values of $\chi \in \{C, \ell, R_g\}$. (b) Spearman's correlation coefficients r_s between the polarization speed v and each network property $\chi \in \{C, \ell, R_g\}$.

162 Transition from simple to complex contagion in consensus models

163 In the previous section, we showed that with the classical LTM, the transition from simple to complex
 164 contagion can be analyzed and understood from a new angle—the speed of contagion—using v as an
 165 indicator of such speed. The question now is whether such a transition can be observed with other
 166 collective decision-making processes that do not involve binary state-variables with cascades of changes,
 167 nor nonlinear mechanisms /thresholds. Specifically, we consider the canonical linear time-invariant
 168 Taylor model^{30,42,43}, which has been widely used to characterize a vast breadth of collective behav-
 169 iors^{1,11,37,38,53,54} and decision making^{30,55}. In the Taylor model, the agents (nodes) seek to reach a
 170 consensus by performing some average of their own state along with those of their neighbors in the
 171 network sense. However, flocking birds and schooling fish in the wild seldom reach a complete consensus
 172 given their incessant collective maneuvering: the convergence to a stationary state clearly does not apply
 173 to their dynamics. This is even more true when these animal groups are dealing with predator attacks
 174 or other external perturbations. Indeed, accumulating empirical evidence shows that swift behavioral
 175 propagation is the true hallmark of collective behavior, rather than high consensus or polarization³⁷. It can
 176 therefore be said that although consensus is at the root of their collective actions, these systems effectively
 177 tend to operate away from consensus^{11,12}.

Considering the particular Taylor model corresponding to the LFC dynamics, one can drive the system away from consensus by imposing a given dynamics to the “leader” (also known as “stubborn”, “zealot”,

“informed” agent in some contexts³⁰). The leader’s behavior then propagates to the neighboring agents, and further to the entire system, thereby determining the emergent collective response. From the control-theoretic perspective, this leader introduces a time-varying input signal into the system. However, this behavioral propagation intricately depends on the network topology, as well as on the leader-follower consensus dynamics considered. Here, we consider N agents with state-variable $x_i(t)$ seeking to follow the arbitrary trajectory $x_0(t) = u(t) = \sin \omega t$ of the leader agent $i = 0$, by means of the following linear distributed consensus:

$$\frac{dx_i}{dt} = \sum_{j=1}^N w_{ij}x_j(t) + w_{i0}u(t), \quad (2)$$

178 where w_{ij} is a weight related to the interaction between agents i and j (Methods). The collective frequency
 179 response of the system, $H^2(\omega)$ (Eq. (7) in Methods), can be interpreted as the number of agents that are
 180 able to respond or follow the leader’s behavior, as a function of its frequency ω ^{11,56}.

181 The LFC dynamics at low frequency ($\omega \rightarrow 0$) has been comprehensively studied. For instance, it is
 182 well known that the collective response increases as ℓ decreases^{14,43,57}. This phenomenology is analogous
 183 to that of a simple contagion (cf. the increase of the polarization speed v as ℓ decreases for the LTM at low
 184 threshold θ , Fig. 1(a)). Given the transition from a simple to a complex contagion when increasing θ in
 185 the LTM, one is naturally led to consider the possible existence of a transition in the LFC when increasing
 186 the frequency ω of the leader’s dynamics.

187 To investigate if the LFC indeed exhibits such a transition, we follow the same approach as for the LTM.
 188 We analyze the collective response on networked systems having 240 nodes with a fixed average degree
 189 of $\langle k \rangle = 16$. Using the same family of small-world WS networks⁵ (Methods), we are able to compute
 190 analytically $H^2(\omega)$ (Fig. 2(a)) for the same values of the clustering C as the ones previously used for the
 191 LTM (Fig. 1). It is worth adding that similar results are obtained with a family of scale-free networks
 192 (Supplementary Fig. S4). Unsurprisingly, at low frequency ($\omega \lesssim 10^{-2}$) we observe a phenomenology
 193 consistent with a simple contagion, namely H^2 increases as ℓ decreases. Upon increasing ω , this trend is
 194 reversed and H^2 grows with C in ways that are reminiscent of a complex contagion. However, to ascertain
 195 that this phenomenology is indeed a transition from a simple to a complex contagion, one has to verify
 196 that the simple contagion at low frequency is driven by ℓ or R_g , while the complex one at high frequency
 197 is controlled by C . To this aim, we calculate the Spearman’s correlation coefficient r_s between H^2 and
 198 $\chi \in \{C, \ell, R_g\}$ (Fig. 2(b)). For these three network metrics, r_s exhibits a clear sigmoidal trend from -1 at
 199 low frequency to $+1$ at high frequency. This trend echoes the one observed with the LTM when varying
 200 θ (Fig. 1(b)), with a transition region in the middle. Let us note that the important element here is the
 201 presence of a transition regardless of the actual values of the upper (resp. lower) bound of the simple (resp.
 202 complex) contagion region. Although beyond the scope of this study, a thorough analysis of the profound
 203 nature of this transition—e.g., cross-over, phase transition—might help in systematically defining the
 204 extent of this transition region.

205 However, we are still unable to conclude that C is fully responsible for the observed trend at high
 206 frequency with the LFC, although this fact is well known for the LTM at high θ . To reach this conclusion,
 207 we have to address a well-known structural constraint with the WS networks, namely the fact that they are
 208 constructed by means of a single parameter—the rewiring probability p ^{5,58,58}. This is clearly visible in
 209 the insert of Fig. 2(b), where C monotonically increases with R_g and ℓ (see Supplementary Fig. S9). To
 210 overcome this issue, we include additional WS networks—with different values of the average degree—and
 211 select a subsample of these networks having uncorrelated network metrics (Methods and insert of Fig. 2(c)).
 212 Given this extended network sampling, we need to account for the effects of degree variations^{12,59,60},

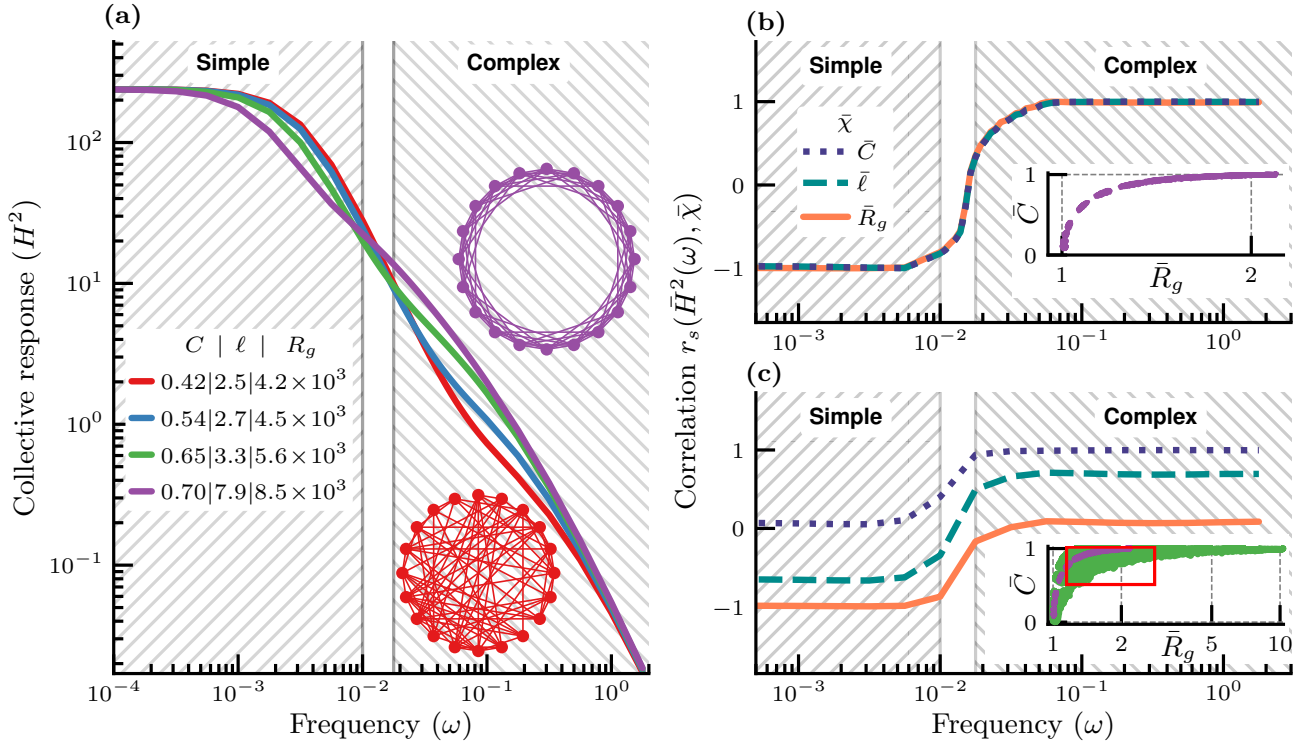


Figure 2. Leader-follower consensus model on WS networks of $N = 240$ nodes. The collective response is averaged over all nodes as leader. **(a)** Collective response H^2 , for a subset of the networks with average degree $\langle k \rangle = 16$; **(b-c)** Spearman's correlation coefficient r_s between the collective response \bar{H}^2 and normalized network metrics $\bar{\chi} \in \{\bar{C}, \bar{\ell}, \bar{R}_g\}$. **(b)** Networks with average degree $\langle k \rangle = 16$. **(c)** Networks with degrees $\langle k \rangle \in \{4, 6, \dots, 32\}$, limited to a range of uncorrelated network parameters. Note that the inserts show the distribution of the normalized clustering coefficients \bar{C} and Kirchhoff indexes \bar{R}_g used to compute r_s (Supplementary Figs. S5–S6). The purple points in the inserts are for networks with $\langle k \rangle = 16$, while those in green in panel (c) are for other values of $\langle k \rangle$. The red box in the insert of panel (c) highlights the dots corresponding to the subsample of networks used to generate the Spearman's correlation coefficient in panel (c), with $r_s(\bar{C}, \bar{R}_g) \approx 0.03$ (Supplementary Fig. S3 for other possible subsampling of networks).

213 and as such we impose a normalization procedure (overbar notation) for all quantities of interest: \bar{H}^2 ,
214 \bar{C} , $\bar{\ell}$ and \bar{R}_g (Methods). Using this methodology, we obtain the following key result: at low frequency,
215 \bar{H}^2 is highly (negatively) correlated with \bar{R}_g and practically uncorrelated with \bar{C} , while the opposite is
216 true at high frequency. This unambiguously confirms our hypothesis that the consensus-based behavioral
217 propagation at low (resp. high) frequency is of the simple (resp. complex) contagion type.

218 It is worth emphasizing that the only commonality between the LTM and the LFC is that both constitute
219 a collective decision-making protocol exhibiting a transition from simple to complex contagion. Although
220 there are obvious similarities between the phenomenology of this transition in both cases—as illustrated
221 by the behaviour respectively of the polarization speed (Fig. 1) and of the collective response (Fig. 2), we
222 do not seek here to establish any formal equivalence between their respective control parameters (θ for the
223 LTM and ω for the LFC).

224 **Complex contagion with networked robots governed by nonlinear heading consensus**

225 The theoretical result described above, concerning the canonical LFC, is compelling in several ways. First,
226 it reveals the existence of a transition from simple to complex contagion in the absence of threshold-based
227 mechanisms. This transition in the behaviour of consensus-based decision-making processes occurs
228 when varying the inherent pace of the behavior that is propagated through the system. Second, it has
229 significant ramifications for the understanding of some collective behaviors subjected to external fast-pace
230 perturbations, e.g., following a predator’s attack leading to collective evasive maneuvers by schools of
231 fish or flocks of birds. As recently stressed by Firth¹⁸, the profound nature of these socially transmittable
232 behaviors has yet to be fully understood. Firth makes clear that the concept of complex contagion has
233 been relatively overlooked by biologists, although it might help explain a vast breadth of collective animal
234 behaviors¹⁸. In addition, there has been emerging evidence of complex contagion in some schooling
235 behaviors of golden shiners exhibiting highly clustered interaction networks². As already mentioned,
236 dealing with wild animal groups is not only challenging from the practical standpoint, but it also restricts
237 the ability to analyze the influence of the deeply-ingrained nature of the interaction among agents.

238 The use of robotic systems—in lieu of biological ones—has been considered to overcome some of
239 these challenges and to offer a new toolkit to deepen our understanding of collective animal behaviors^{40,41}.
240 Although simulations offer unique ways to systematically analyze algorithms of collective dynamics, they
241 inevitably reduce the fidelity of the model to achieve computational tractability. Indeed, the simulation-
242 reality gap in robotics is known to be exacerbated with multi-robot systems⁶¹. For instance, simulations
243 can fail to adequately capture: (1) the complex physical interactions among agents, (2) the inherent
244 variability among units forming the group, and (3) the fine details of real-world settings in which the
245 agents are embedded. As a matter of fact, achieving high-fidelity simulations often requires the input or
246 feedback from physical experiments.

247 Data gathered *in robotico*, with a highly controllable and controlled environment, enable a rapid inves-
248 tigation of a number of hypotheses about collective behaviors. In turn, the outcome of such investigations
249 can serve biologists to identify new directions to explore, test and validate with empirical data. Following
250 this strategy, we use a networked robotic system to assess various socially transmittable behaviors when
251 changing the topology of the interaction network in the presence of a collective decision-making with a
252 nonlinear component. It is worth stressing that the results obtained with the LFC (Fig. 2) are for a linear
253 system dynamics, yet they reveal a surprisingly complex phenomenology. Nonetheless, some collective
254 decision-making processes among moving animals are based on a consensus associated with the direction
255 of travel, and are inherently nonlinear. Such nonlinear interactions among conspecifics have recently been
256 shown to be responsible for sudden directional switches in groups of pigeons⁶².

257 Therefore, we carried out a series of experiments on nonlinear leader-follower heading consensus with

258 a collective of ground robots where each one aligns its direction of travel with that of their neighbors in
 259 the network sense (Methods). As a consequence, changing the structure of the interaction network—and
 260 in particular its properties such as $\chi \in \{C, \ell, R_g\}$ —modifies the nature of the neighborhoods involved in
 261 the nonlinear heading consensus. This type of collective decision-making—closely related to Vicsek’s
 262 canonical model of collective motion⁶³—bears some resemblance with the Taylor model analyzed previ-
 263 ously. However, a physical embodiment of such a complex system involves significant deviations from
 264 the ideal scenario corresponding to the theoretical calculations obtained for the LFC. For instance, while
 265 the dynamics of the robots are ultimately governed by physical processes that are continuous in time, the
 266 units sense each other’s state using asynchronous, discrete communications with stochastic delays and
 267 communications dropouts¹².

268 The networked robotic system comprises 10 robots (1 leader and 9 followers, Methods) equipped with
 269 a “swarm-enabling” unit—providing on-board data-processing, computing and distributed communication
 270 capabilities—that allows the system to perform a collection of decentralized cooperative control strate-
 271 gies⁶⁴. The leader continuously rotates at a fixed frequency ω in the range $0.03 \text{ Hz} < \omega \leq 0.3 \text{ Hz}$. Each
 272 robot, including the leader, periodically transmits its heading information to its direct neighbors as per the
 273 specific network topology considered. Three distinct topologies (“Random”, “Ring” and “Caveman” as
 274 shown at the bottom of Fig. 3) are selected on the basis that they have the same average degree $\langle k \rangle = 4$,
 275 yet notably different clustering coefficients C (Methods).

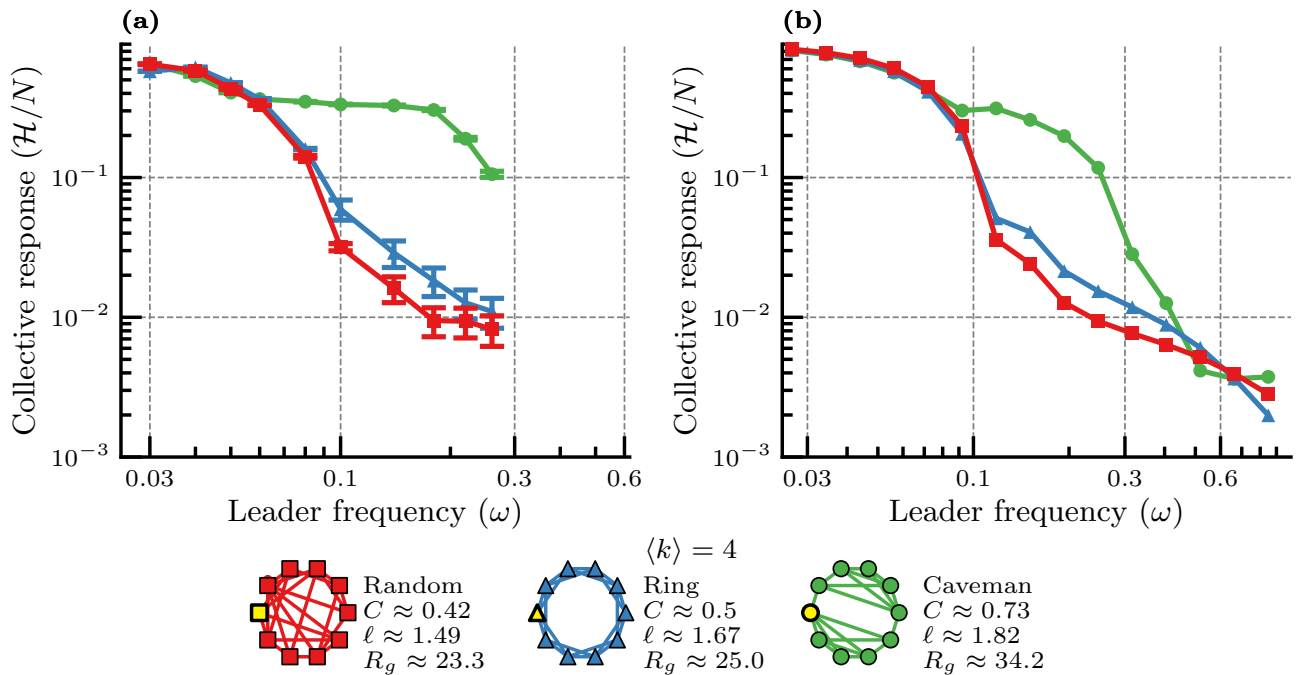


Figure 3. Experimental analysis with a leader-follower networked robotic system networked by means of three topologies: “Random”, “Ring” and “Caveman” with $\langle k \rangle = 4$ and $9 + 1$ agents (Methods). The graphs represent the network topologies used in the series of experiments, with the selected leader node depicted in yellow: (a) Experimental results of angular consensus dynamics (mean value and associated standard deviation; Methods), (b) simulation results of the nonlinear angular consensus dynamics.

276 It is worth highlighting that this experimental setup and methodology are identical to the one reported

277 in Ref.¹², except for the fact that different network topologies are considered here. According to the
278 analysis of the LFC, the collective response of this networked robotic system is expected to go down when
279 increasing the frequency ω of the leader agent. This appears clearly in Fig. 3(a) for all three networks
280 considered. The decrease in the collective response is essentially the same at low frequency ($\omega \leq 0.06$ Hz)
281 for all cases. Above that frequency however, we observe a strong difference between all 3 topologies in
282 the range $0.06 \text{ Hz} \leq \omega \leq 0.2 \text{ Hz}$. This intermediate range of frequencies shows a rich collective behavior
283 since the dynamics of the leader is rather “fast” thereby preventing any form of heading consensus to be
284 achieved. This places us in a regime similar to that of animal groups dealing with fast-pace perturbations.
285 Beyond 0.2 Hz, the highest collective response, achieved with the “Caveman” network, experiences a
286 sharper decline, which we suspect would go down to the same low level as for the “Random” and “Ring”
287 networks at higher frequencies. Unfortunately, increasing the frequency above 0.3 Hz is not possible in
288 practice due to a limit in the achievable rotation frequency of the leader.

289 To compensate for this experimental limitation, we perform simulations of the leader-follower non-
290 linear heading consensus dynamics with $9 + 1$ agents by integrating the system of Eqs. (15) (Fig. 3(b)).
291 Unsurprisingly, these simulations show higher levels of collective response at low frequency, compared to
292 the experimental ones, as they correspond to an idealized communication between agents. In addition,
293 the frequency at which the differences between the different networks become apparent is higher in the
294 simulation case with respect to the experimental one. Finally, we can reach higher frequency in the
295 simulations than in the experiments, and the results do show the expected merging of the three collective
296 responses at the highest frequency values (that were not reached in Fig. 3(a)).

297 Following the analytical results with the LFC (Fig. 4), we are able to further analyze the robotic
298 experiments. The complex contagion induced by the leader unit to the 9 followers is clearly visible in the
299 intermediate frequency range $0.06 \text{ Hz} \leq \omega \leq 0.2 \text{ Hz}$. The results are indeed in excellent agreement with
300 the complex contagion phenomenology studied previously in much larger networks (“complex” hatched
301 region of Fig. 4(a)). When the robotic units are interconnected by means of the most clustered network
302 (“Caveman”), the behavioral spread is the most effective and the collective response the highest. On
303 the other hand, when decreasing the clustering between robotic units—from “Caveman” to “Ring” and
304 ultimately to “Random”—the effectiveness of the spread of the leader’s behavior is reduced, and so is the
305 ensuing collective response at the group level.

306 We note on the other hand that, given that the experiment is limited to 10 robotic units with an average
307 degree $\langle k \rangle = 4$, the diameters and Kirchhoff indices for all 3 networks are small. Therefore, the simple
308 contagion process at low frequency ($\omega \leq 0.06$ Hz) is simply too rapid and no meaningful distinction
309 between the considered topologies can be observed experimentally (Fig. 3(a)).

310 Discussion

311 In summary, we have shown theoretically and experimentally that complex contagions are more general
312 and prevalent than originally thought, and that transitions from simple to complex contagion are not
313 limited to threshold-based models. Instead, our results suggest that such a transition might be a general
314 feature in some classes of collective decision-making processes.

315 Network science has been instrumental in uncovering the existence of complex contagions by Centola
316 & Macy^{13,16} in the social sciences. Since these seminal works, complex contagions have been observed
317 in other spreading dynamics over complex networks, including epidemic-like stochastic models^{22–25}.
318 However, and as already mentioned, the study of the transition from simple to complex contagion has
319 still been limited to the original LTM used by Centola & Macy, as well as social network experiments
320 with binary options in decision-making. Hence, our discovery of this very transition within a fully linear

321 decision-making protocol devoid of any thresholds greatly expands the relevance of this phenomenon to a
322 vast breadth of collective decision-making processes beyond the social sciences, and including collective
323 animal behavior and collective robotics.

324 At this point, it is critical to realize that ascertaining the exact nature of a contagion—simple or
325 complex—remains challenging. Because of that, some scientists still cautiously use the term “complex
326 contagion” or even refer to it obliquely: e.g., “complex contagion flavor”⁶⁵. Even with the full details of:
327 (1) a given collective dynamics—e.g, linear threshold dynamics for a given value of θ , or a leader-follower
328 consensus dynamics for a given value of ω —as well as (2) the interaction network topology among
329 agents, one is lacking a definite way of characterizing the behavioral contagion. This work offers a key
330 conceptual advance in overcoming this challenge. Indeed, the network-based classification proposes to
331 vary the topology with the goal of either increasing or reducing both the clustering coefficient C and
332 the Kirchhoff index R_g . In the event that the effectiveness of the behavioral propagation is found to be
333 positively correlated with C and uncorrelated with R_g , then the contagion is complex. Conversely, if a
334 behavioral propagation is negatively correlated with R_g and uncorrelated with C , then it can be classified as
335 a simple contagion (Fig. 2(c)). It is therefore worth stressing that this complex networks characterization
336 of simple/complex contagions is agnostic to the actual details of the collective decision-making process.
337 In all cases investigated here, the simple or complex nature of a behavioral propagation is determined by
338 the value of a control parameter of the dynamical process taking place at the node level: e.g., the threshold
339 θ for the LTM and the inherent pace of the behavior ω for the LFC. The proposed characterization allows
340 us to identify the intervals of the control parameter associated with simple or complex contagions, with a
341 transition region in between (Figs. 1 & 2).

342 Despite the apparent relative simplicity of this complex networks characterization of contagions, one
343 should not underestimate the associated practical challenges for scientists studying a specific collective
344 decision-making dynamics among humans, within animal groups, or with networked robots. Varying
345 the network topology might not always be achievable as previously stressed in the case of flocks of
346 birds or schools of fish. This approach was central to Centola’s study of humans involved in an online
347 social experiment, in which the topology of the social network was controlled and manipulated²⁰. This
348 groundbreaking experiment has been made possible thanks to the emergence of online social networks and
349 the related technology. Clearly, such an approach could not be considered and implemented with animal
350 groups. However, as our networked robotic experiment shows, the use of artificial agents mimicking
351 animal behaviors offers a new toolkit to analyze and gain insight into collective animal behavior. With this
352 approach, one can carry out the proposed complex networks characterization and ascertain the nature—
353 simple or complex—of the behavioral propagation. Last but not least, one can also modify the triggering
354 behavior—in our experiment the stimulus associated with the frequency of the leader—to possibly uncover
355 a transition from simple to complex contagion. Such an approach opens new doors toward understanding
356 the mechanisms underpinning such collective behaviors.

357 Given how ubiquitous collective decision-making is in human societies, animal groups and networked
358 multi-agent systems, these new results will have profound ramifications for our understanding of numerous
359 phenomena in these fields. The importance of these results goes beyond the class of consensus-based proto-
360 cols considered here, although studying a second-order leader-follower consensus⁶⁶ with an underdamped
361 dynamics seems like a natural extension to this work given its acknowledged relevance to collective
362 information transfer in flocks of birds^{36,37}. The novelty of these results effectively has implications for a
363 vast breadth of collective decision-making protocols involving a continuum of options to choose from.
364 Firth¹⁸ recently speculated the importance of complex contagions in animal social networks and behavioral
365 contagions. Interestingly, Rosenthal et al.² had the intuition that complex contagions occur in schools of
366 golden shiners owing to the high levels of clustering exhibited by their network of interaction. This led

367 them to consider a (fractional) threshold-based model—generating complex contagions—to characterize
 368 behavioral cascades in this particular schooling setting². While Rosenthal et al. limited their work to
 369 threshold-based models to analyze this phenomenon, our results would allow their study to be expanded
 370 upon, as the decision-making process in golden shiners is clearly based on a continuum of options. From
 371 the same research group and with the same animal groups, Sosna et al. provided additional empirical
 372 evidence about the importance of the topology of the interaction network on collective responsiveness³.
 373 They also speculate that the fish might actively control their interactions to achieve a higher collective
 374 responsiveness³. Our results offer a theoretical backing to this idea, and it might provide biologists with
 375 new directions to explore and experiment.

376 Besides shedding a new light on our understanding of collective behaviors, these results have also clear
 377 implications for the design of man-made networked systems: e.g., Internet of Things, multi-robot systems,
 378 dynamic sensor networks. Finally, we hope the present analysis of these rich phenomena of transition
 379 from simple to complex contagion will be extended to more complex networks, including heterogeneous,
 380 temporal and/or multi-layer networks.

381 **Methods**

382 ***Linear threshold model***

The LTM is a binary-option model of collective decision-making widely used in the study of complex
 contagion^{13,16}. As described in Refs.^{16,17,27}, it consists of a connected network of N nodes, with each node
 i characterized by a state-variable with two possible discrete values $s_i(t) \in \{0, 1\}$ —inactive or active—and
 a fixed threshold value $\theta_i \in [0, 1]$. At $t = 0$, all nodes start in the inactive state except for a random seed
 node l and its neighbors, denoted by $\{j | j \sim l\}$, whose state is set to active. Whenever the fraction of
 an agent's neighbors that are in the active state is larger than or equal to the agent's threshold θ_i , that
 node will switch to the active state, i.e. $s_i(t + 1) = 1$ when $\langle s_{j \sim i}(t) \rangle \geq \theta_i$. The LTM dynamics on a given
 network can be characterized by the average polarization or activity, defined as $P(t) = \langle s_i(t) \rangle_{\{i=1, \dots, N\}}$,
 and the associated polarization speed^{11,46}

$$v(t) = \frac{P(t) - P(0)}{t}, \quad (3)$$

383 which effectively is the average propagation speed until instant t .

384 Note that when $P(t) = 1$, all nodes are in the active state and a global cascade has taken place.
 385 Particular emphasis has been put on characterizing which network topologies lead to global cascades for
 386 certain values of θ_i ^{13,16,17}, and the realisation that complex contagions spread faster on networks with
 387 high levels of clustering^{16,20,45}. However, numerous empirical observations attest that behavioral cascades
 388 are rarely global: evasive maneuvers in schooling golden shiners involve 10 ~ 30% of the individuals²
 389 and the adoption of new health behavior in an online social network experiment only reached 30 ~ 60% of
 390 participants²⁰. Since complex contagions exhibit faster spreading in their early stage of propagation^{20,45}
 391 that in their late near-global stage, we focus here on the early dynamics of the cascade and therefore
 392 consider the polarization speed $v(t_f)$ for which 30% of the nodes are activated, i.e. for the smallest time t_f
 393 where $P(t_f) > 0.3$ (Supplementary Fig. S1 for other cascade sizes).

394 To study the transition from simple to complex contagion with the LTM, we consider fairly large
 395 networks of $N = 10^4$ nodes, with identical thresholds $\theta_i = \theta \forall i$, in order to ensure that the active state
 396 propagates for long enough at low values of θ . We let the active state propagate from a randomly selected
 397 seed node and its neighbors until the system reaches equilibrium where $P(t_{\text{end}} + 1) = P(t_{\text{end}})$. In our
 398 analysis we only consider networks where $P(t_{\text{end}})$ is at least as large as the desired cascade size, and we
 399 omit from our analysis the simulations where the active state failed to propagate.

400 **Leader-follower consensus model**

The leader-follower consensus model (LFC)^{11,12,42}—a particular version of the Taylor model³⁰— is commonly used by the control community to study opinion dynamics and formation control. Here, N identical agents perform a distributed consensus protocol on their state-variable $x_i(t)$, and one particular agent $i = 0$ —the leader—follows an arbitrary trajectory $x_0(t) = u(t)$ instead. The dynamics of this linear system is governed by the following set of first-order ODEs:

$$\frac{dx_i}{dt} = \sum_{j=1}^N w_{ij}x_j(t) + w_{i0}u(t), \quad (4)$$

where $w_{ij} = \omega_0(a_{ij}/k_i - \delta_{ij})$ is the inter-agent consensus protocol weight for the interaction between agents i and j . The natural response frequency ω_0 is assumed to be the same for all agents. The degree of agent i is given by $k_i = \sum_{j=0}^N a_{ij}$, and the adjacency matrix entry is $a_{ij} = 1$ if agent i is connected to j and 0 otherwise—classically δ_{ij} is the Kronecker delta. The solution to Eq. (4) in the frequency domain can be expressed in matrix form as¹²

$$\mathbf{X}(\omega) = (j\omega\mathbf{I} - \mathbf{W}_F)^{-1}\mathbf{W}_L u(\omega), \quad (5)$$

with \mathbf{I} the appropriately sized identity matrix, $\mathbf{W}_F = (w_{ij})_{N \times N} = \omega_0\mathbf{L}_G$ where \mathbf{L}_G is the grounded Laplacian matrix⁴² and $\mathbf{W}_L = (w_{i0})_{\{i=1,\dots,N\}}$ is the consensus protocol between the N followers and the leader $i = 0$. The frequency response of the multi-agent system measures the ability of the agents to follow the leader's trajectory, $u(t)$, and can be expressed in the frequency domain as the transfer function along the $j\omega$ axis in the s -plane^{12,67}

$$\mathbf{H}(\omega) = \left(\frac{\delta\mathbf{X}}{\delta u} \right) (\omega) = (j\omega\mathbf{I} - \mathbf{W}_F)^{-1}\mathbf{W}_L, \quad (6)$$

with the entries of the vector $\mathbf{H} = (h_i)_{\{i=1,\dots,N\}}$ corresponding to the individual agent's frequency response. It is clear from Eq. (6) that the response function has a nontrivial dependency on the topology of the agents' connectivity through the adjacency matrix, and therefore the entries of \mathbf{W}_F and \mathbf{W}_L . We define the collective frequency response of the system as¹²

$$H^2(\omega) = \mathbf{H}^\dagger(\omega)\mathbf{H}(\omega) = \sigma^2(\omega), \quad (7)$$

401 with \dagger being the adjoint matrix operator and σ being the singular value of the system with a single
 402 leader—classically used in the analysis of multiple-input and multiple-output (MIMO) systems. When
 403 all agents in the system perfectly follow the leader's behavior the response reaches its maximum value,
 404 $H^2 = N$. Thus the quantity H^2/N can be interpreted as the fraction of agents in the system following the
 405 leader. It is worth stressing that since H^2 is not constant under leader selection, the results we present in
 406 this paper are obtained by averaging over all possible leader placements in the network.

407 To study the transition from simple to complex contagion in the LFC, we consider networks of
 408 $N + 1 = 240$ agents. This is significantly smaller than for the LTM, but the LFC shows a much higher
 409 sensitivity to variations in the network metrics, which yields a range of H^2 large enough to perform our
 410 analysis, even with relatively small network sizes.

411 **Networks and metrics**

412 To study the influence of the network topology on the behavioral propagation in the LTM and the LFC, we
 413 use the small-world Watts–Strogatz (WS) network model⁵. These networks enable us to vary key network

414 metrics by changing a single parameter, namely the rewiring probability⁵ p . To quantify the generated
 415 network topologies, we use the following metrics: the clustering coefficient C , the average shortest path ℓ
 416 and the Kirchhoff Index R_g defined below. We use an average degree $\langle k \rangle = 16$ for Fig. 1 and Fig. 2(a–b)
 417 to ensure high levels of C before rewiring⁶⁰ and a large range in ℓ and R_g .

418 **Clustering coefficient**

419 To measure the level of community structure, and thus the potential for reinforcement of the behavior that
 420 is propagating, we use the average of the local clustering coefficient as defined in Ref.⁵, and we simply
 421 refer to it as “clustering coefficient” or C throughout the paper.

422 **Average shortest path**

423 The shortest path between a given pair of nodes is the minimum number of hops needed to connect the
 424 two. The average shortest path is the average between all pairs of nodes. It is well known that for WS
 425 networks, decreasing the distance between nodes both increases the effectiveness of simple contagion^{5,16}
 426 and the time it takes to reach consensus¹⁴.

427 **Kirchhoff index**

The Kirchhoff index R_g —also known as the resistance distance—is a distance metric obtained by replacing
 every connection with a $1\ \Omega$ resistor and averaging the resistance between all node pairs⁵⁹, thus considering
 all paths on the network. Further, R_g is directly related to the eigenvalues $0 = \lambda_1 < \lambda_2 < \dots < \lambda_N$ of the
 Laplacian matrix⁵⁹ and can be expressed as

$$R_g = N \sum_{i=2}^N \frac{1}{\lambda_i}. \quad (8)$$

428 The cohesion of the follower states—under a white noise disturbance—can be measured by the H_∞ -norm
 429 of the dynamics of Eq. (4)—which is $H^2(\omega = 0)$ —and it has been proven that maximizing the cohesion is
 430 done by minimizing the Kirchhoff index R_g ^{42,43}.

431 **Correlations**

We consider the Spearman’s rank correlation r_s to investigate the impact of network metrics on a given
 collective behavior. We use the rank correlation due to the expected nonlinear relationship between the
 performance of the collective behavior and network metrics for both the LTM and LFC^{12,14} (Supplementary
 Figs. S2, S5 & S6 for point distributions). The Spearman’s correlation is defined by

$$r_s = \frac{\text{cov}(\text{rg}_X, \text{rg}_Y)}{\text{std}(\text{rg}_X)\text{std}(\text{rg}_Y)}, \quad (9)$$

432 with rg_X being the rank of the metric, $\text{cov}(X)$ and $\text{std}(X)$ the covariance and standard deviation respectively.

Given the fact that the WS networks are generated by varying one single free parameter (the rewiring
 probability p), the associated network metrics are inevitably correlated. As a consequence, we are unable
 to distinguish the individual effects of each network metric for a given average degree $\langle k \rangle$ (insert of
 Fig. 2(b)). To overcome this, we generate networks of different average degrees $k \in \{4, 6, \dots, 32\}$, and
 consider a sampled set of these networks for which C and R_g vary independently of each other (insert of
 Fig. 2(c)). However, as shown in Refs.^{11,12}, the collective frequency response H^2 is notably influenced by
 the degree distribution, and so are the network metrics considered $\chi \in \{C, \ell, R_g\}$ ^{14,59,60}. To account for
 that degree dependency, we normalize all quantities involved, with the normalized quantity denoted by an

overbar. First, the normalized collective frequency response is given by

$$\bar{H}^2(\omega, k, p) = \frac{H^2(\omega, k, p)}{H^2(\omega, k, p_{\max})}, \quad (10)$$

in which $p_{\max}(\omega, k)$ is the rewiring probability that yields the largest $H^2(\omega, k, p)$. Note that $\bar{H}^2(\omega) \leq 1$. Second, the normalized clustering coefficient is defined as

$$\bar{C}(k, p) = \frac{C(k, p)}{C(k, p = 0)}, \quad (11)$$

such that for any k the most clustered networks, obtained for $p = 0$, have $\bar{C} = 1$ (Supplementary Fig. S5). Third, since the distance metrics also change with $\langle k \rangle$ ^{14,59}, we introduce the following normalized distance metrics

$$\bar{\ell}(k, p) = \frac{\ell(k, p)}{\ell(k, p = 1)}, \quad (12)$$

$$\bar{R}_g(k, p) = \frac{R_g(k, p)}{R_g(k, p = 1)}, \quad (13)$$

433 which are based on the smallest distances, obtained with $p = 1$.

434 From all the networks generated with different p and $\langle k \rangle$, we construct a sample that almost fully
 435 decorrelates the clustering coefficient and the Kirchhoff index: i.e., such that $r_s(\bar{C}, \bar{R}_g) \approx 0$ (insert of
 436 Fig. 2(c), and Supplementary Fig. S3 for other subsamples of networks).

437 **Nonlinear heading consensus experiments**

438 To empirically measure the collective response—with differently paced leaders—we use the same experi-
 439 mental multi-robot setup as Ref.¹² with $N = 10$ robotic units (called ‘eBots’) communicating by means of
 440 their so-called “swarm enabling unit”⁶⁴. These ground differential-drive robots are collectively moving
 441 about a two-dimensional domain (Supplementary Fig. S10). The motion of the units is the superposition of
 442 a translational motion and a rotational one. In this setup, the leader agent undergoes a constant rotational
 443 motion such that its heading $\alpha_L(t)$ is governed by $\frac{d\alpha_L(t)}{dt} = \omega$, with ω denoting the frequency of the leader.
 444 Its ‘leader’ status comes from the fact that its behavior does not depend on the follower agents. Note that
 445 the agents have no way of distinguishing the leader from any other agent in the system.

The robot’s heading is the only state-variable driven by the robot’s controller regardless of the speed. Specifically, the $N_F = 9$ follower eBots seek to align their heading $\alpha_i(t)$ with that of their neighbors $\alpha_{j \sim i}(t)$. The nonlinear heading consensus algorithm determines a target heading $\bar{\alpha}$ for each unit according to

$$\bar{\alpha}_i = \langle \alpha \rangle_{j \sim i} = \arctan \left(\frac{\sum_{j \sim i} \sin \alpha_j}{\sum_{j \sim i} \cos \alpha_j} \right), \quad (14)$$

where $j \sim i$ denotes the set of topological neighbors of i in the network sense, and $\langle \cdot \rangle$ is an angular average. The nonlinear heading consensus (14) is identical to the one considered in Vicsek’s model⁶³ except for the fact that we use a static topological neighborhood while a metric one was originally considered in Ref.⁶³. Each follower unit updates its target heading $\bar{\alpha}_i$ asynchronously every $\Delta T = 0.1$ s. The nonlinear heading consensus algorithm used in the experiments is a discrete-time equivalent of

$$\frac{d\alpha_i}{dt} = \omega_0 (\langle \alpha \rangle_{j \sim i} - \alpha_i), \quad (15)$$

446 with $\omega_0 \Delta T \gg 1$ and for times $t \gg \Delta T$. Here, ω_0 is the natural frequency of angular rotation of the eBots.
447 The information of each neighbor's state is also updated with the same sampling rate, but not necessarily
448 concurrently with each other or with the update of Eq. (14).

449 The robots are interconnected according to three fixed network topologies with $\langle k \rangle = 4$ due to size
450 limitations of the network $N = 10$, namely: the connected caveman network⁵⁸ (for maximal clustering
451 coefficient), a k -regular random network (for low values of C), and the 1D ring lattice (WS networks with
452 $p = 0$ offering an intermediate level of C). These three fixed network topologies provide a wide range of
453 values for the clustering coefficient as shown in Fig. 3.

Each run of the experiment starts at $t = 0$ with all eBots aligned with the leader: i.e., $\alpha_i(0) = \alpha_L(0) = 0 \forall i$. Each run lasts for a duration of $T = 10$ minutes to make sure the leader performs a meaningful number of rotations for all frequencies considered. The capacity of the N_F followers to maintain their heading aligned with that of the leader is measured by the empirical collective response¹²

$$\mathcal{H} = \sum_{i=1}^{N_F} \frac{1}{T} \int_0^T \cos(\alpha_i(t) - \alpha_L(t)) dt, \quad (16)$$

454 which is averaged over three repeated runs, for each angular speed of the leader considered.

455 References

- 456 1. Swain, D. T., Couzin, I. D. & Leonard, N. E. Coordinated speed oscillations in schooling killi-
457 fish enrich social communication. *J. Nonlinear Sci.* **25**, 1077–1109, DOI: <http://doi.org/10.1007/s00332-015-9263-8> (2015).
- 459 2. Rosenthal, S. B., Twomey, C. R., Hartnett, A. T., Wu, H. S. & Couzin, I. D. Revealing the hidden
460 networks of interaction in mobile animal groups allows prediction of complex behavioral contagion.
461 *Proc. Natl. Acad. Sci.* **112**, 4690–4695, DOI: <http://doi.org/10.1073/pnas.1420068112> (2015).
- 462 3. Sosna, M. M. G. et al. Individual and collective encoding of risk in animal groups.
463 *Proc. Natl. Acad. Sci.* **116**, 20556–20561, DOI: <http://doi.org/10.1073/pnas.1905585116> (2019).
- 464 4. Centola, D. *How Behavior Spreads: The Science of Complex Contagions* (Princeton University
465 Press, 2018).
- 466 5. Watts, D. J. & Strogatz, S. H. Collective dynamics of ‘small-world’ networks. *Nature* **393**, 440–442,
467 DOI: <http://doi.org/10.1038/30918> (1998).
- 468 6. Kinney, R., Crucitti, P., Albert, R. & Latora, V. Modeling cascading failures in the North American
469 power grid. *The Eur. Phys. J. B* **46**, 101–107, DOI: <http://doi.org/10.1140/epjb/e2005-00237-9>
470 (2005).
- 471 7. Koç, Y., Warnier, M., Van Mieghem, P., Kooij, R. E. & Brazier, F. M. The impact of the topology on
472 cascading failures in a power grid model. *Phys. A* **402**, 169–179, DOI: <http://doi.org/10.1016/j.physa.2014.01.056> (2014).
- 474 8. Ren, W. & Beard, R. W. *Distributed Consensus in Multi-Vehicle Cooperative Control*, vol. 27
475 (Springer, 2008).
- 476 9. Kwa, H. L., Kit, J. L. & Bouffanais, R. Optimal
477 swarm strategy for dynamic target search and tracking. In
478 *Proceedings of the 19th International Conference on Autonomous Agents and MultiAgent Systems*,
479 672–680, DOI: <http://doi.org/http://ifaamas.org/Proceedings/aamas2020/pdfs/p672.pdf> (Richland, SC,
480 2020).

- 481 **10.** Barrat, A., Barthelemy, M. & Vespignani, A. Dynamical Processes on Complex Networks (Cam-
482 bridge University Press, Leiden, 2008).
- 483 **11.** Mateo, D., Kuan, Y. K. & Bouffanais, R. Effect of correlations in swarms on collective response.
484 Sci. Reports **7**, 10388, DOI: <http://doi.org/10.1038/s41598-017-09830-w> (2017).
- 485 **12.** Mateo, D., Horsevad, N., Hassani, V., Chamanbaz, M. & Bouffanais, R. Optimal network topology
486 for responsive collective behavior. Sci. Adv. **5**, eaau0999, DOI: <http://doi.org/10.1126/sciadv.aau0999>
487 (2019).
- 488 **13.** Centola, D. & Macy, M. W. Complex contagions and the weakness of long ties. Am. J. Sociol. **113**,
489 702–734, DOI: <http://doi.org/10.1086/521848> (2007).
- 490 **14.** Olfati-Saber, R. Ultrafast consensus in small-world networks. In
491 Proceedings of the 2005, American Control Conference, 2371–2378, DOI: <http://doi.org/10.1109/acc.2005.1470321> (2005).
- 493 **15.** Santos, F. C. & Pacheco, J. M. Scale-free networks provide a unifying framework for the emergence of
494 cooperation. Phys. Rev. Lett. **95**, 098104, DOI: <http://doi.org/10.1103/physrevlett.95.098104> (2005).
- 495 **16.** Centola, D., Eguíluz, V. M. & Macy, M. W. Cascade dynamics of complex propaga-
496 tion. Phys. A: Stat. Mech. its Appl. **374**, 449–456, DOI: <http://doi.org/10.1016/j.physa.2006.06.018>
497 (2007).
- 498 **17.** Watts, D. J. A simple model of global cascades on random networks. Proc. Natl. Acad. Sci. **99**,
499 5766–5771, DOI: <http://doi.org/10.1073/pnas.082090499> (2002).
- 500 **18.** Firth, J. A. Considering complexity Animal social networks and behavioural contagions.
501 Trends Ecol. & Evol. **35**, 100–104, DOI: <http://doi.org/10.1016/j.tree.2019.10.009> (2020).
- 502 **19.** Romero, D. M., Meeder, B. & Kleinberg, J. Differences in the mechanics of information
503 diffusion across topics: idioms, political hashtags, and complex contagion on twitter. In
504 Proceedings of the 20th international conference on World wide web, 695–704, DOI: <http://doi.org/10.1145/1963405.1963503> (2011).
- 506 **20.** Centola, D. The spread of behavior in an online social network experiment. Science **329**, 1194–1197,
507 DOI: <http://doi.org/10.1126/science.1185231> (2010).
- 508 **21.** Törnberg, P. Echo chambers and viral misinformation: Modeling fake news as complex contagion.
509 PLOS one **13**, e0203958, DOI: <http://doi.org/10.1371/journal.pone.0203958> (2018).
- 510 **22.** Karsai, M., Iñiguez, G., Kaski, K. & Kertész, J. Complex contagion process in spreading of online
511 innovation. J. The Royal Soc. Interface **11**, 20140694, DOI: <http://doi.org/10.1098/rsif.2014.0694>
512 (2014).
- 513 **23.** Dodds, P. S. & Watts, D. J. Universal behavior in a generalized model of contagion. Phys. Rev. Lett.
514 **92**, 218701, DOI: <http://doi.org/10.1103/physrevlett.92.218701> (2004).
- 515 **24.** Böttcher, L., Luković, M., Nagler, J., Havlin, S. & Herrmann, H. J. Failure and recovery in dynamical
516 networks. Sci. Reports **7**, 41729, DOI: <http://doi.org/10.1038/srep41729> (2017).
- 517 **25.** Böttcher, L., Nagler, J. & Herrmann, H. J. Critical behaviors in contagion dynamics. Phys. Rev. Lett.
518 **118**, 088301, DOI: <http://doi.org/10.1103/physrevlett.118.088301> (2017).
- 519 **26.** Andreoni, J., Nikiforakis, N. & Siegenthaler, S. Predicting social tipping and norm change in
520 controlled experiments. Proc. Natl. Acad. Sci. **118**, DOI: <http://doi.org/10.1073/pnas.2014893118>
521 (2021).

- 522 **27.** Granovetter, M. Threshold models of collective behavior. Am. J. Sociol. **83**, 1420–1443, DOI:
523 <http://doi.org/10.1086/226707> (1978).
- 524 **28.** Friedkin, N. E., Proskurnikov, A. V., Tempo, R. & Parsegov, S. E. Network science on belief system
525 dynamics under logic constraints. Science **354**, 321–326, DOI: <http://doi.org/10.1126/science.aag2624>
526 (2016).
- 527 **29.** Tian, Y. et al. Social power evolution in influence networks with stubborn individuals.
528 IEEE Transactions on Autom. Control. **nil**, 1–1, DOI: <http://doi.org/10.1109/tac.2021.3052485>
529 (2021).
- 530 **30.** Proskurnikov, A. V. & Tempo, R. A tutorial on modeling and analysis of dynamic social networks.
531 part i. Annu. Rev. Control. **43**, 65–79, DOI: <http://doi.org/10.1016/j.arcontrol.2017.03.002> (2017).
- 532 **31.** Handegard, N. O. et al. The dynamics of coordinated group hunting and collective information transfer
533 among schooling prey. Curr. Biol. **22**, 1213–1217, DOI: <http://doi.org/10.1016/j.cub.2012.04.050>
534 (2012).
- 535 **32.** Couzin, I. D., Krause, J. et al. Self-organization and collective behavior in vertebrates.
536 Adv. Study Behav. **32**, 10–1016 (2003).
- 537 **33.** Krause, J. & Ruxton, G. D. Living in Groups (Oxford University Press, 2002).
- 538 **34.** Kastberger, G., Schmelzer, E. & Kranner, I. Social waves in giant honeybees repel hornets. PLoS ONE
539 **3**, e3141, DOI: <http://doi.org/10.1371/journal.pone.0003141> (2008).
- 540 **35.** Radakov, D. V. Schooling in the Ecology of Fish (J. Wiley, 1973).
- 541 **36.** Attanasi, A. et al. Information transfer and behavioural inertia in starling flocks. Nat. Phys. **10**,
542 691–696, DOI: <http://doi.org/10.1038/nphys3035> (2014).
- 543 **37.** Cavagna, A., Giardina, I. & Grigera, T. S. The physics of flocking: Correlation as a compass from
544 experiments to theory. Phys. Reports **728**, 1–62, DOI: <http://doi.org/10.1016/j.physrep.2017.11.003>
545 (2018).
- 546 **38.** Attanasi, A. et al. Collective behaviour without collective order in wild swarms of midges.
547 PLOS Comput. Biol. **10**, e1003697, DOI: <http://doi.org/10.1371/journal.pcbi.1003697> (2014).
- 548 **39.** Cavagna, A. et al. Flocking and turning: a new model for self-organized collective motion.
549 J. Stat. Phys. **158**, 601–627, DOI: <http://doi.org/10.1007/s10955-014-1119-3> (2014).
- 550 **40.** Li, L. et al. Vortex phase matching as a strategy for schooling in robots and in fish. Nat. Commun.
551 **11**, 5408, DOI: <http://doi.org/10.1038/s41467-020-19086-0> (2020).
- 552 **41.** Li, L., Ravi, S., Xie, G. & Couzin, I. D. Using a robotic platform to study the in-
553 fluence of relative tailbeat phase on the energetic costs of side-by-side swimming in fish.
554 Proc. Royal Soc. A: Math. Phys. Eng. Sci. **477**, rspa.2020.0810, DOI: [http://doi.org/10.1098/rspa.](http://doi.org/10.1098/rspa.2020.0810)
555 [2020.0810](http://doi.org/10.1098/rspa.2020.0810) (2021).
- 556 **42.** Pirani, M., Shahrivar, E. M. & Sundaram, S. Coherence and convergence rate in networked dynamical
557 systems. In 2015 54th IEEE Conference on Decision and Control (CDC), 968–973, DOI: <http://doi.org/10.1109/cdc.2015.7401998>
558 (2015).
- 559 **43.** Baumann, F., Sokolov, I. M. & Tyloo, M. A laplacian approach to stubborn agents and their
560 role in opinion formation on influence networks. Phys. A: Stat. Mech. its Appl. **557**, 124869, DOI:
561 <http://doi.org/10.1016/j.physa.2020.124869> (2020).

- 562 **44.** Zhong, Y. D. & Leonard, N. E. A continuous threshold model of cascade dynamics. In
563 2019 IEEE 58th Conference on Decision and Control (CDC), 1704–1709, DOI: <http://doi.org/10.1109/cdc40024.2019.9029844> (2019).
564
- 565 **45.** O’Sullivan, D. J. P., O’Keeffe, G. J., Fennell, P. G. & Gleeson, J. P. Mathematical modeling of complex
566 contagion on clustered networks. Front. Phys. **3**, 71, DOI: <http://doi.org/10.3389/fphy.2015.00071>
567 (2015).
- 568 **46.** Peng, H., Nematzadeh, A., Romero, D. M. & Ferrara, E. Network modularity controls the speed of
569 information diffusion. Phys. Rev. E **102**, 052316, DOI: <http://doi.org/10.1103/physreve.102.052316>
570 (2020).
- 571 **47.** Barthelemy, M., Barrat, A., Pastor-Satorras, R. & Vespignani, A. Dynamical patterns of epidemic
572 outbreaks in complex heterogeneous networks. J. Theor. Biol. **235**, 275–288, DOI: <http://doi.org/https://doi.org/10.1016/j.jtbi.2005.01.011> (2005).
573
- 574 **48.** Karsai, M. et al. Small but slow world: How network topology and burstiness slow down spreading.
575 Phys. Rev. E **83**, 025102, DOI: <http://doi.org/10.1103/physreve.83.025102> (2011).
- 576 **49.** Delvenne, J., Lambiotte, R. & Rocha, L. E. C. Diffusion on networked systems is a question of time
577 or structure. Nat. Commun. **6**, 7366, DOI: <http://doi.org/10.1038/ncomms8366> (2015).
- 578 **50.** Starnini, M., Machens, A., Cattuto, C., Barrat, A. & Pastor-Satorras, R. Immunization strategies
579 for epidemic processes in time-varying contact networks. J. Theor. Biol. **337**, 89–100, DOI: <http://doi.org/https://doi.org/10.1016/j.jtbi.2013.07.004> (2013).
580
- 581 **51.** Lawyer, G. Understanding the influence of all nodes in a network. Sci. Reports **5**, 8665, DOI:
582 <http://doi.org/10.1038/srep08665> (2015).
- 583 **52.** Holme, P. & Rocha, L. E. C. Impact of misinformation in temporal network epidemiology. Netw. Sci.
584 **7**, 52–69, DOI: <http://doi.org/10.1017/nws.2018.28> (2019).
- 585 **53.** Young, G. F., Scardovi, L., Cavagna, A., Giardina, I. & Leonard, N. E. Starling flock networks
586 manage uncertainty in consensus at low cost. PLOS Comput. Biol. **9**, e1002894, DOI: <http://doi.org/10.1371/journal.pcbi.1002894> (2013).
587
- 588 **54.** Vicsek, T. & Zafeiris, A. Collective motion. Phys. Reports **517**, 71–140, DOI: <http://doi.org/10.1016/j.physrep.2012.03.004> (2012).
589
- 590 **55.** Amelkin, V., Bullo, F. & Singh, A. K. Polar opinion dynamics in social networks.
591 IEEE Transactions on Autom. Control. **62**, 5650–5665, DOI: <http://doi.org/10.1109/TAC.2017.2694341> (2017).
592
- 593 **56.** Mastroeni, L., Vellucci, P. & Naldi, M. Agent-based models for opinion formation: a bibliographic
594 survey. IEEE Access **7**, 58836–58848, DOI: <http://doi.org/10.1109/access.2019.2913787> (2019).
- 595 **57.** Olfati-Saber, R., Fax, J. A. & Murray, R. M. Consensus and cooperation in networked multi-agent
596 systems. Proc. IEEE **95**, 215–233, DOI: <http://doi.org/10.1109/jproc.2006.887293> (2007).
- 597 **58.** Watts, D. J. Networks, dynamics, and the small-world phenomenon. Am. J. Sociol. **105**, 493–527,
598 DOI: <http://doi.org/10.1086/210318> (1999).
- 599 **59.** Ellens, W., Spijksma, F., Van Mieghem, P., Jamakovic, A. & Kooij, R. E. Effective graph resistance.
600 Linear Algebr. its Appl. **435**, 2491–2506, DOI: <http://doi.org/10.1016/j.laa.2011.02.024> (2011).

- 601 **60.** Kooij, R. E., Horsevad, N. S. & Bouffanais, R. Tuning the clustering coefficient of generalized
602 circulant networks. *Phys. A: Stat. Mech. its Appl.* **578**, 126088, DOI: <http://doi.org/https://doi.org/10.1016/j.physa.2021.126088> (2021).
603
- 604 **61.** Dorigo, M., Theraulaz, G. & Trianni, V. Swarm robotics: Past, present, and future. *Proc. IEEE* **109**,
605 1152–1165, DOI: <http://doi.org/10.1109/jproc.2021.3072740> (2021).
- 606 **62.** Chen, D. et al. Coordinating directional switches in pigeon flocks: the role of nonlinear interactions.
607 *Royal Soc. Open Sci.* **8**, nil, DOI: <http://doi.org/10.1098/rsos.210649> (2021).
- 608 **63.** Vicsek, T., Czirók, A., Ben-Jacob, E., Cohen, I. & Shochet, O. Novel type of phase transition in a
609 system of self-driven particles. *Phys. Rev. Lett.* **75**, 1226, DOI: <http://doi.org/10.1103/PhysRevLett.75.1226> (1995).
610
- 611 **64.** Chamanbaz, M. et al. Swarm-enabling technology for multi-robot systems. *Front. Robotics AI* **4**, 12,
612 DOI: <http://doi.org/10.3389/frobt.2017.00012> (2017).
- 613 **65.** Iacopini, I., Petri, G., Barrat, A. & Latora, V. Simplicial models of social contagion. *Nat. Commun.*
614 **10**, 2485, DOI: <http://doi.org/10.1038/s41467-019-10431-6> (2019).
- 615 **66.** Punzo, G., Young, G. F., Macdonald, M. & Leonard, N. E. Using network dynamical influence to
616 drive consensus. *Sci. Reports* **6**, 26318, DOI: <http://doi.org/10.1038/srep26318> (2016).
- 617 **67.** Ogata, K. *Modern Control Engineering* (Prentice Hall, 2010).

618 **Acknowledgements (not compulsory)**

619 This work is partially supported by the National Research Foundation (NRF) under its National Cyberse-
620 curity R&D Programme (Award No. NRF2014NCR-NCR001-040). The authors also acknowledge the
621 support from the SUTD-MIT International Design Center under the Grant #IDG31900101. A.B. is partially
622 supported by the Agence Nationale de la Recherche (ANR) project DATAREDUX (ANR-19-CE46-0008).

623 **Author contributions statement**

624 N.H., D.M. and R.B. designed the study and the experiment. N.H. and D.M. developed the analytical and
625 numerical tools. D.M. and R.B. conceived the experiments. N.H. conducted the numerical calculations
626 and simulations. A.B., R.E.K, D.M., R.B and N.H. analyzed the data and results. N.H. conducted the
627 experiments. All authors wrote and reviewed the manuscript.

628 **Competing interests**

629 The authors declare no competing interests

630 **Data availability**

631 All data needed to evaluate the conclusions in the paper are present in the paper and/or the Supplementary
632 Information. Additional data related to this paper may be requested from the authors.

633 **Code availability**

634 All codes developed for this study are available at [https://github.com/Horsevad/Simple_to_](https://github.com/Horsevad/Simple_to_complex_contagion_in_collective_decision-making)
635 [complex_contagion_in_collective_decision-making](https://github.com/Horsevad/Simple_to_complex_contagion_in_collective_decision-making)

636 **Supplementary Information**

637 Supplementary Information accompanies this paper.